Article

Cite This: Biomacromolecules 2019, 20, 243−253

pubs.acs.org/Biomac

Inhibiting Bacterial Adhesion by Mechanically Modulated Microgel Coatings

Damla Keskin,[†] Olga Mergel,*[,†] Henny C. van der Mei,[†] Henk J. Busscher,[†] and Patrick van Rijn*[,†,‡]

[†]University of Groningen, University Medical Center Groningen, Department of Biomedical Engineering (FB40), W.J. Kolff Institute for Biomedical Engineering and Materials Science (FB41), Antonius Deusinglaan 1, 9713 AV Groningen, The Netherlands

[‡]University of Groningen, Zernike Institute for Advanced Materials, Nijenborgh 4, 9747 AG Groningen, The Netherlands

Supporting Information

ABSTRACT: Bacterial infection is a severe problem especially when associated with biomedical applications. This study effectively demonstrates that poly-*N*-isopropylmethacrylamide based microgel coatings prevent bacterial adhesion. The coating preparation via a spraying approach proved to be simple and both cost and time efficient creating a homogeneous dense microgel monolayer. In particular, the influence of cross-linking density, microgel size, and coating thickness was investigated on the initial bacterial adhesion. Adhesion of *Staphylococcus aureus* ATCC 12600 was imaged using a parallel plate flow chamber setup, which gave insights in the number of the total bacteria adhering per unit area onto the surface and the initial bacterial deposition rates. All microgel coatings successfully yielded more than 98% reduction in bacterial adhesion. Bacterial adhesion depends both on the cross-linking density/stiffness of the microgels and on the thickness of the microgel coating. Bacterial adhesion decreased when a lower cross-linking density was used at equal coating thickness and at equal cross-linking density with a thicker microgel coating. The highest reduction in the number of bacterial adhesion was achieved with the microgel that produced the thickest coating (h = 602 nm) and had the lowest cross-linking density. The results provided in this paper indicate that microgel coatings serve as an interesting and easy applicable approach and that it can be fine-tuned by manipulating the microgel layer thickness and stiffness.

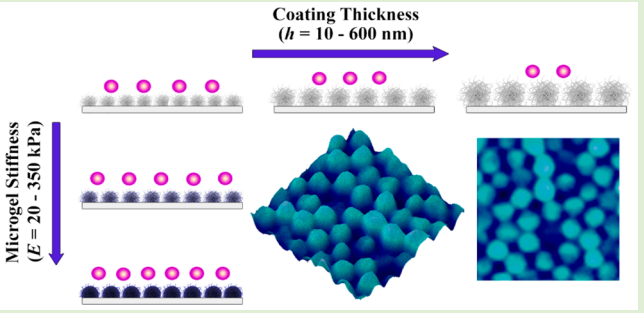

INTRODUCTION

Bacterial adhesion on surfaces negatively affects a wide range of applications such as medical implants and biomedical devices,[1−4] biosensors,[5,6] water purification plants,[7,8] food packaging,[9] marine and industrial materials.[10−12] Particularly, bacterial adhesion and biofilm formation on a biomaterial implant surface can create biomaterial related infections and subsequently serious health risks to patients. Adhering and growing bacterial colonies rapidly produce a matrix of extracellular polymeric substances (EPS) on the implant surface, which shields against antibiotics and the host immune system. Accordingly, biofilms on implant surfaces are more difficult to treat with antibiotics compared to planktonic bacteria. Consequently, surgical removal of infected implants is often required and is causing a lot of pain for the patients and costs for healthcare.[13,14]

Initial bacterial adhesion is related to the surface properties of the solid surface and influenced by many factors such as hydrophobicity,[15] roughness,[16] charge[17] and stiffness.[18] To minimize the initial bacterial adhesion and to gain control of the biomaterial surface characteristics via surface modification has been a long-standing approach. Hence, different surface modification methods, such as polymer brush coatings,[19,20] polyethylene glycol (PEG)-based coatings[21,22] or self-assembled monolayers (SAMs),[23] have been used to enhance the fouling resistance. Although these methods improve the nonfouling behavior of the surface, they have drawbacks in terms of stability and cytotoxicity. Covalently attached polymer brushes require a complicated synthesis setup and the use of Fe or Cu catalysts is not desirable for biomedical applications.[24] The stability of SAMs on gold substratum, including alkanethiol-based ones, are also limited due to, e.g., the thiolate oxidation that is occurring even under ambient environmental conditions.[25] On the other hand, the long-term stability of poly(ethylene oxide) (PEO) and (PEG)-based coatings still needs to be developed further.[26]

Recently, microgel coatings attracted increasing attention to inhibit cellular[27−29] or protein adhesion[29] onto surfaces. Microgels are water-swollen, cross-linked spherical polymeric particles, with the ability to undergo a volume phase transition (VPT) upon environmental alterations.[30−33] When the chemical composition is chosen carefully, microgels are able to respond to external stimuli such as temperature,[33,34] pH,[34]

Special Issue: Biomacromolecules BPC

Received: September 14, 2018
Revised: December 2, 2018
Published: December 4, 2018

DOI: 10.1021/acs.biomac.8b01378
Biomacromolecules 2019, 20, 243−253

Scheme 1. Schematic Illustration of Bacterial Adhesion on Microgel-Coated Surfaces as Function of Microgel Stiffness and Coating Thickness[a]

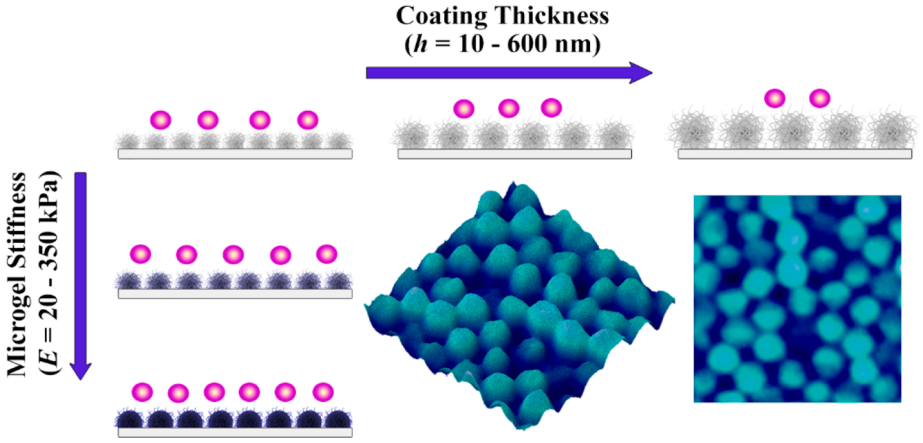

[a]Decreased bacterial adhesion for softer microgel coatings; thick and soft coatings are most efficient in their antifouling performance.

light,[31] electric field,[35] solvent composition,[36] inducing conformational changes. Based on their stimuli responsiveness and excellent properties such as softness, porosity, elasticity, water storage capacity[27] combined with good biocompatibility[37] these "intelligent" hydrogels attracted tremendous interest in material science owing to their potential applications in biomedical technologies, as controlled drug delivery,[36,38] and tissue engineering[39] but also in catalysis,[40] photonics,[41] purification technologies,[33,42] and sensing.[43]

Microgels offer a robust and facile approach for surface modification and microgel-based coatings have been used to prevent mammalian cells (10−100 μm) and proteins (4−150 kDa) from adhering to the coatings.[27,29,44−49] The hydrogel and highly hydrated state of these kinds of coatings are presumably a major contributor to the antifouling effects although the presence of specific chemistry may further influence or facilitate these effects. Heparin-mimicking microgels composed of poly(acrylicacid-*co*-*N*-vinyl-2-pyrrolidone) (P(AA-VP)) and poly(2-acrylamido-2-methylpropanesulfonic acid-*co*-acrylamide) (P(AMPS-AM)) decreased the amount of adsorbed protein with more than 50% when applied as a coating on a membrane surface.[50] Also, zwitterionic−dopamine copolymer microgel coatings showed distinct antifouling performance toward proteins on a wide spectrum of different materials such as glass, mica and gold.[51] While proteins and mammalian cells have been studied on microgels, adhesion of bacteria has not been investigated so far. In addition, the full potential of the microgel coating has not yet been explored as microgels offer the opportunity to introduce various physicochemical as well as (bio)chemical functionalities.[52]

One of the tunable physicochemical microgel properties is the microgel stiffness, and it is known that the mechanical properties of a material influence the adhesion of eukaryotic cells.[27] Although, it was recently demonstrated that bacterial adhesion is affected by stiffness and coating thickness of homogeneous bulk-like hydrogels,[53,54] bacterial adhesion to microgels and their altering mechanical properties and size features has not yet been studied. Moreover, microgels have a much larger surface to volume ratio and exhibit remarkably faster swelling/deswelling transition rates compared to their macroscopic counterparts, which is advantageous for many types of applications such as drug delivery, biomaterials, chemical separation and catalysis.[27,55,56]

In the present study, we use poly-*N*-isopropylmethacrylamide, P(NIPMAM) based microgels as antifouling coatings and evaluate the decoupled relationship between microgel coating stiffness and thickness on bacterial adhesion properties. The P(NIPMAM) microgel building blocks with easy controllable predetermined characteristics were adsorbed on glass substrata by a simple, cost- and time-efficient spraying deposition technique based on electrostatic interactions, with polyethylenimine (PEI) as an anchoring polymer.[27] One of the main advantages of this type of bottom-up approach compared to more elaborate synthetic approaches (e.g., surface-initiated polymerization) is the easy tunability of microgel properties providing a versatile approach for the design of surfaces with predetermined characteristics such as thickness, stiffness, porosity and functionality. The mechanical properties of microgels were evaluated by atomic force microscopy (AFM) in the hydrated state. Bacterial adhesion studies were conducted using nonmotile Gram-positive *Staphylococcus aureus* ATCC 12600 as a model microbe. By combination of well-controllable P(NIPMAM) microgel design parameters (functionality, thickness and stiffness), we have created a powerful scaffold to systematically evaluate how bacterial adhesion is affected by the thickness or microgel internal cross-linking concentration (*N*,*N*′-methylenebis(acrylamide), BIS). Hence, we successfully evaluated the influence of these parameters and gained new insight to enhance the non-fouling surface characteristics for possible biomedical applications (Scheme 1).

MATERIALS AND METHODS

Materials. *N*-Isopropylmethacrylamide (97%, NIPMAM), the cross-linker *N*,*N*′-methylenebis(acrylamide) (99%, BIS), the surfactant sodium dodecyl sulfate (SDS), the initiator ammonium persulfate (98% APS) and polyethylenimine (PEI, branched, Mw 25.000 g/mol) were purchased from Sigma-Aldrich, Zwijndrecht, The Netherlands. The dyes methacryloxyethyl thiocarbamoyl rhodamine B (MRB) and Nile blue acrylamide (NBA) were purchased from Polysciences, Inc., Hirschberg, Germany. *N*-Isopropylmethacrylamide was recrystallized from hexane; all other chemicals were used as received without any further purification. Ultrapure water (18.2 MΩ, arium 611 DI water purification system; Sartorius AG, Göttingen, Germany) was used in all experiments.

Synthesis of P(NIPMAM) Microgel. In a three-necked 100 mL flask equipped with a flat anchor-shaped mechanical stirrer, a reflux condenser and a nitrogen in- and outlet, 604 mg (4.8 mmol, 95 mol %)

DOI: 10.1021/acs.biomac.8b01378
Biomacromolecules 2019, 20, 243−253

Table 1. Molar Composition of the P(NIPMAM) Microgel Reaction Mixture and the Initial Weight of the Components

	monomer (NIPMAM)			cross-linker (BIS)			surfactant (SDS)		initiator (APS)	
	initial weight [mg]	molar amount [mmol]	molar content [mol %]	initial weight [mg]	molar amount [mmol]	molar content [mol %]	initial weight [mg]	molar concentration [mM]	initial weight [mg]	molar amount [mmol]
μGel1	626	4.93	98.5	12	0.08	1.5	23	1.6	11	0.05
μGel2	604	4.75	95	39	0.25	5	23	1.6	11	0.05
μGel3	541	4.25	85	116	0.75	15	23	1.6	11	0.05
μGel4	626	4.93	98.5	12	0.08	1.5	0	0	11	0.05
μGel5	604	4.75	95	39	0.25	5	10	0.7	11	0.05
μGel6	626	4.93	98.5	12	0.08	1.5	2	0.2	11	0.05

of NIPMAM, 39 mg (0.25 mmol, 5 mol %) of BIS, 10 mg of MRB (0.02 mmol, 0.3 mol %) and 23 mg (1.6 mM) of SDS were dissolved in 45 mL of water, and the reaction mixture was degassed with N_2 for 1 h. The solution was heated to 70 °C and the reaction was started by injecting the degassed initiator solution of 11 mg (0.05 mmol) APS in 5 mL water into the reaction mixture. After 10 min, opalescence appeared, and the reaction was continued for another 4 h at 70 °C and 300 rpm under N_2 atmosphere. The reaction mixture was cooled to room temperature and stirred overnight. The microgel dispersion was purified by ultracentrifugation followed by decantation and dispersion of the sediment in water (3 times at 179.200 g). The product, P(NIPMAM) μGel, was freeze-dried after purification for further use. The synthesis was carried out via the same procedure for all microgels with slight adjustment of the reaction mixture composition, which is indicated in Table 1.

Surface Preparation/Microgel Coating. A glass slide (Menzel GmbH, Braunschweig, Germany, 76 mm × 26 mm × 1 mm) was rinsed with ethanol (70%) and water and subsequently dried with pressurized air. Plasma oxidation was performed for 10 min (at 100 mTorr and 0.2 mbar, on Plasma Active Flecto 10 USB). The glass slide was immersed in PEI solution for 20 min (1.5 mg/mL, 0.15 wt %, while the pH was adjusted to pH 7 with 0.1 M HCl solution) and afterward rinsed three times with water. After drying at room temperature, a microgel suspension (5 mg/mL, 0.5 wt %) was sprayed onto the PEI modified glass slide (tilted 45°) until the whole surface is wetted (8−12 times) to coat the surface. The spraying device used is a glass bottle with a spray nozzle, which assists the microgel suspension to transform from a liquid into a spray in order to disperse the liquid evenly over the area of the substrate. Specific volume for one spray burst of this spraying bottle is about 140 μL. 8 up to 12 times spraying means 1.1 mL up to 1.7 mL of microgel suspension sprayed to the surface. The coated surface was dried first at room temperature and subsequently overnight in the oven at 50 °C. The slides with the dried microgel (multi) layer were immersed in water for at least 6 h while the water was replaced three times. The washing step assures that only microgels that are physically bound to the PEI surface remain attached and create a homogeneous monolayer.

EXPERIMENTAL TECHNIQUES

Dynamic Light Scattering (DLS). The hydrodynamic radius, R_h, and particle size distribution experiments of the microgels were performed on a Zetasizer Nano-ZS (Malvern Instruments, Worcestershire, U.K.). Temperature-dependent measurements were recorded at a fixed scattering angle of 173° and a wavelength λ = 633 nm of the laser beam while the temperature was varied in the range of 30 to 60 °C at 2 °C intervals and with a measurement time of 10 s and 11 runs, performed in triplicates. The samples were highly diluted to avoid multiple scattering. For data evaluation, the cumulant fit analysis was used and the hydrodynamic radius Rh was calculated by use of the Stokes−Einstein equation.

Zeta (ζ) Potential Measurements. Electrophoretic mobility measurements were performed on a Zetasizer Nano-ZS (Malvern Instruments, Worcestershire, U.K.) in disposable capillary cells (Malvern, DTS1070) in water. Electrophoretic mobility was measured at an angle of 17° and a wavelength λ = 633 nm of the laser beam. The ζ-potential was calculated from the electrophoretic mobility by use of the Smoluchowski equation.

Atomic Force Microscopy. Surface morphology of the microgel coated glass slides was determined with AFM (Dimension 3100 Nanoscope V, Veeco, Plainview, NY, USA) in contact mode using DNP cantilevers (spring constant k = 0.06 N/m, or k = 0.24 N/m and resonant frequency f_0 = 18 kHz, or f_0 = 56 kHz) made from silicon nitride in dry and wet state.

To study single adsorbed microgels, 20 μL of a 0.025 wt % microgel suspension was spin coated (60 s at 81 ps) onto a plasma activated silicon wafer, and AFM measurements were performed in their hydrated state. Quantitative analysis of the single absorbed microgel properties was performed on a Catalyst Nanoscoop V instrument (Bruker, Billerica, MA, USA) using the PeakForce QNM (quantitative nanomechanical mapping) mode of Bruker with a large amplitude in fluid. Bruker SCANASYST-FLUID silicon nitride cantilevers (k = 0.7 N/m, f_0 = 120−180 kHz,) with nominal tip (r = 20 nm) were used. The system was calibrated before each measurement by determining the exact spring constant and deflection sensitivity of the tip in fluid for the determination of the elastic modulus. The force curves were fitted with the Hertz model,

$$F = \frac{4}{3}\left(\frac{E}{1-\vartheta^2}\right)\sqrt{R}\,\delta^{3/2}$$

with F = force, E = Young's modulus, R = tip radius, υ = Poisson's ratio and δ = indentation to extract the elastic modulus E from the force mapping data. The given elastic modulus represents an average over the entire microgel particle profile, while a minimum amount of 5 particles was used for calculation. The NanoScope Analysis software was used for data evaluation.

Bacterial Strain and Growth Conditions. *S. aureus* ATCC 12600 was used in this study. The strain was first grown overnight at 37 °C on an agar plate from a frozen stock that was stored in DMSO at −80 °C. Several colonies were used to inoculate 10 mL tryptone soya broth (TSB; Oxoid, Basingstoke, UK). This preculture was then incubated at 37 °C for 24 h and used to inoculate a second culture of 200 mL TSB that was allowed to grow for 16 h. The bacteria from the second culture were harvested by centrifugation at 5000*g* for 5 min at 10 °C and washed with potassium phosphate buffered saline (PBS, 10 mM potassium phosphate, 0.15 M NaCl, pH 7.0). Following this, bacteria were sonicated on ice for 30 s at 30 W (Vibra Cell model VCX130; Sonics and Materials Inc., Newtown, CT, USA) in order to obtain single bacteria by breaking bacterial clusters. Subsequently, the bacteria were resuspended in 200 mL PBS solution to a concentration of 3×10^8 bacteria per mL for adhesion experiments, as detected using a Bürker−Türk counting chamber.

Assessment of Bacterial Adhesion. Bacterial adhesion on microgel coated glass surfaces was performed using a custom-built parallel plate flow chamber by flowing bacterial suspension 3×10^8 mL^{-1} for 4 h at room temperature at a set shear rate of 12 s^{-1}, as stated by a protocol previously described.[57,58] Before starting each experiment, PBS was circulated through the flow chamber to remove air bubbles. The dimensions of viewing area of flow chamber system is with a width of 17 mm, length of 67 mm, height of 0.75 mm and the assembly of the flow chamber with a diagram is explained in detail in the Supporting Information (Scheme S1). After 4 h, the flow of the bacterial suspension was stopped and switched to PBS buffer solution at the same flow rate for 30 min in order to remove nonadhering bacteria

DOI: 10.1021/acs.biomac.8b01378
Biomacromolecules 2019, 20, 243−253

from the system. Bacterial adhesion was monitored using a phase-contrast microscope (OlympusBH-2) and live images (1392 × 1040 pixels with 8-bit resolution) were acquired after summation of 15 consecutive images (time interval 1 s) to increase the signal-to-noise ratio and to eradicate moving bacteria from the analysis.

For identifying the numerical values for bacterial adhesion, individual bacteria were counted as follows. Five images at different spots on the coated glass slide were taken after 4 h of bacterial adhesion. The total number of individual bacteria adhering to the surface were counted from these images both manually and by software. The number of bacteria adhering per cm^2 was enumerated using in-house developed software based on MATLAB, when the total number of bacteria was more than ca. 300 and manually when below 300. The number of bacteria per unit area was calculated and compared using one-way Anova comparison tests. Differences were considered significant if $p < 0.05$. Initial deposition rate was calculated from the number of the bacteria adhering during the first 15 min. Images were taken every minute for the first 15 min, and the number of bacteria adhering per cm^2 was enumerated. From the plot of the number of adhering bacteria versus time, the initial deposition rate (j_0, in $cm^{-2}\ s^{-1}$) was calculated by linear regression analysis. Statistical analysis for the initial deposition rate comparisons was done using a two-tailed *t*-test with the Benferroni correction. Differences were considered significant if $p < 0.05$. All values given in this paper are the averages of experiments on three separately microgel coated surfaces and were performed with separately cultured bacteria.

RESULTS AND DISCUSSION

Microgel Synthesis and Characterization. Temperature responsive P(NIPMAM) microgels were prepared by a precipitation polymerization method described earlier.[27] The internal stiffness of the microgels was varied by changing the molar ratio of the cross-linker BIS to the main monomer NIPMAM, see Table 1 for the different compositions. The chosen cross-linker concentration percentages with respect to NIPMAM were 1.5, 5 and 15 mol % of BIS and the synthesis parameters are summarized in Table 1. The microgel stiffness is reflected by the swelling/deswelling ratio (Q; R_h swollen/R_h collapsed), meaning that a larger difference between the swollen state and the collapsed state upon passing the volume phase transition temperature (VPTT), the microgel is regarded as softer due to lower internal cross-linking density. The temperature response of three microgels with very similar hydrodynamic radii R_h, but different cross-linking densities is shown in Figure 1. The VPTT of the P(NIPMAM) microgels is 44 °C and in good agreement with previously reported values.[27] The highly cross-linked, more rigid microgel with 15 mol % of BIS exhibits the lowest swelling ratio of $Q = 1.5$, based on many connection points in the particle interior, which restrict the swelling/deswelling. In contrast, the soft P(NIPMAM) microgel with low cross-linking density shows a swelling ratio of $Q = 2.3$ (see Table 2 and Figure 1).

The deformability, because of different internal cross-linking, is also expected to influence the morphology of the microgel adsorbed onto the surface. Morphological characterization of surface adsorbed microgels was performed by AFM in the wet state (Figure 2) and dry state (Figure S1). As shown in Figure 2, the softer particles, with 1.5 mol % BIS (μGel1; $h = 10 \pm 5$ nm at the particle center) and 5 mol % BIS (μGel2; $h = 13 \pm 3$ nm) reveal a "pancake"-like structure. In contrast, the highly cross-linked P(NIPMAM) particle with 15 mol % BIS (μGel3) exhibits a larger height of $h = 59 \pm 14$ nm due to internal particle stabilization based on the cross-links preventing it from deforming as much as the other particles. The deformability of the microgels adsorbed onto the surface is in good agreement

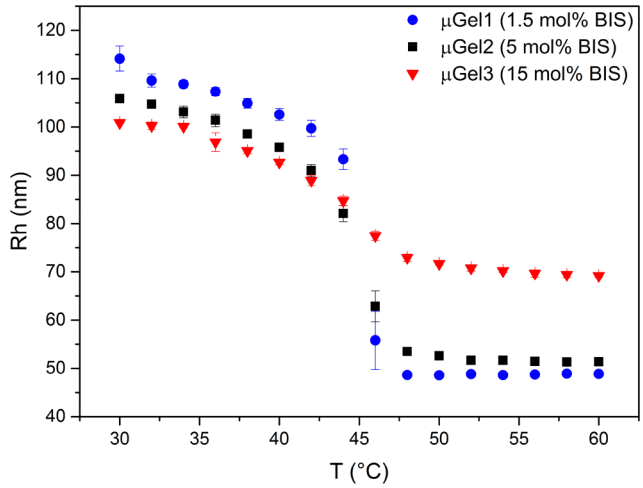

Figure 1. Hydrodynamic radius R_h as a function of the temperature of P(NIPMAM) microgels with different cross-linking densities.

with the microgel stiffness obtained by quantitative nanomechanical mapping AFM experiments. The elastic modulus ranges from 21 ± 8 kPa for the soft particle, with 1.5 mol % BIS (μGel1), over 117 ± 20 kPa for the intermediate stiff microgel, with 5 mol % BIS (μGel2) to 346 ± 125 kPa for the stiff particle with a cross-linking density of 15 mol % BIS (μGel3, see Table 2 and Figure S5). For the intermediate stiff microgel (5 mol % BIS), the quantified values are in good agreement with previously reported values of around 100 kPa and displayed a lateral stiffness gradient profile over the entire particle increasing toward the particle center.[27] This phenomenon is especially pronounced for the stiffer microgel with changes over 1 order of magnitude from 610 kPa at the particle center to 60 kPa at the outer region of the microgel ($\Delta E = 550$ kPa see Figure S5). The changes in elastic modulus are decreasing with increasing deformability and flexibility of the particle, with $\Delta E = 97$ kPa for a cross-linking density of 5 mol % BIS (131 kPa (center) - 34 kPa (periphery)) and $\Delta E = 42$ kPa for the soft microgel (1.5% BIS, 44−2 kPa, see Figure S5). The characteristics of the microgels in solution and at the surface are given in Table 2.

The thickness of the coating, as also indicated previously with bulk hydrogel layers,[53] may play a crucial role in bacterial adhesion. Therefore, microgels with a similar surface adsorbed thickness of $h \approx 60$ nm were synthesized in order to investigate the effect of the stiffness independently from thickness variations. Different amounts of surfactant (SDS) were used to control the final hydrodynamic radius R_h of the microgels.[59] By a stabilization of the growing particles at an early stage of the polymerization, the surfactant prevents particles from growing. Thus, a higher amount of SDS leads to smaller final particle size. The temperature response of these microgels (μGel4, μGel5 and μGel6) is given in the Supporting Information (Figure S2) and the height profile in Figure 2 reveals a similar thickness as the higher cross-linked P(NIPMAM) microgels. The characteristics of all microgels used in this study are summarized in Table 2. This selection of P(NIPMAM) microgels enables elucidation of the particle stiffness (Q-value), size, and coating thickness on the bacterial adhesion in an independent fashion allowing to assess which parameter is most crucial.

For example, the particles depicted in Figure 2A,B,C reveal a comparison of different stiffnesses and similar R_h, but different deformability characteristics of the surface absorbed particles. Microgels shown in Figure 2C,E,F instead show similar surface

DOI: 10.1021/acs.biomac.8b01378
Biomacromolecules 2019, 20, 243−253

Table 2. Characteristics of Surface Adsorbed P(NIPMAM) Microgels and P(NIPMAM) Microgels in Suspension

	molar content of cross-linker BIS [mol %]	Elastic modulus [kPa]	hydrodynamic radius R_h [nm] @ 30 °C	swelling degree/ratio Q	ζ-potential [mV]	height h [nm] of surface adsorbed μgels in dry state	height h [nm] of surface adsorbed μgels in wet state
μGel1	1.5	21 ± 8	114 ± 3	2.3	−13 ± 1	6 ± 1	10 ± 5
μGel2	5	117 ± 20	109 ± 5	2.1	−19 ± 3	12 ± 2	13 ± 3
μGel3	15	346 ± 125	101 ± 1	1.5	−23 ± 1	31 ± 8	59 ± 14
μGel4	1.5	22 ± 7	787 ± 135	2.2	−16 ± 0.4	52 ± 4	602 ± 74
μGel5	5	106 ± 38	301 ± 8	2.1	−18 ± 0.2	30 ± 4	57 ± 8
μGel6	1.5	18 ± 7	650 ± 87	4.8	−11 ± 0.2	25 ± 9	54 ± 26

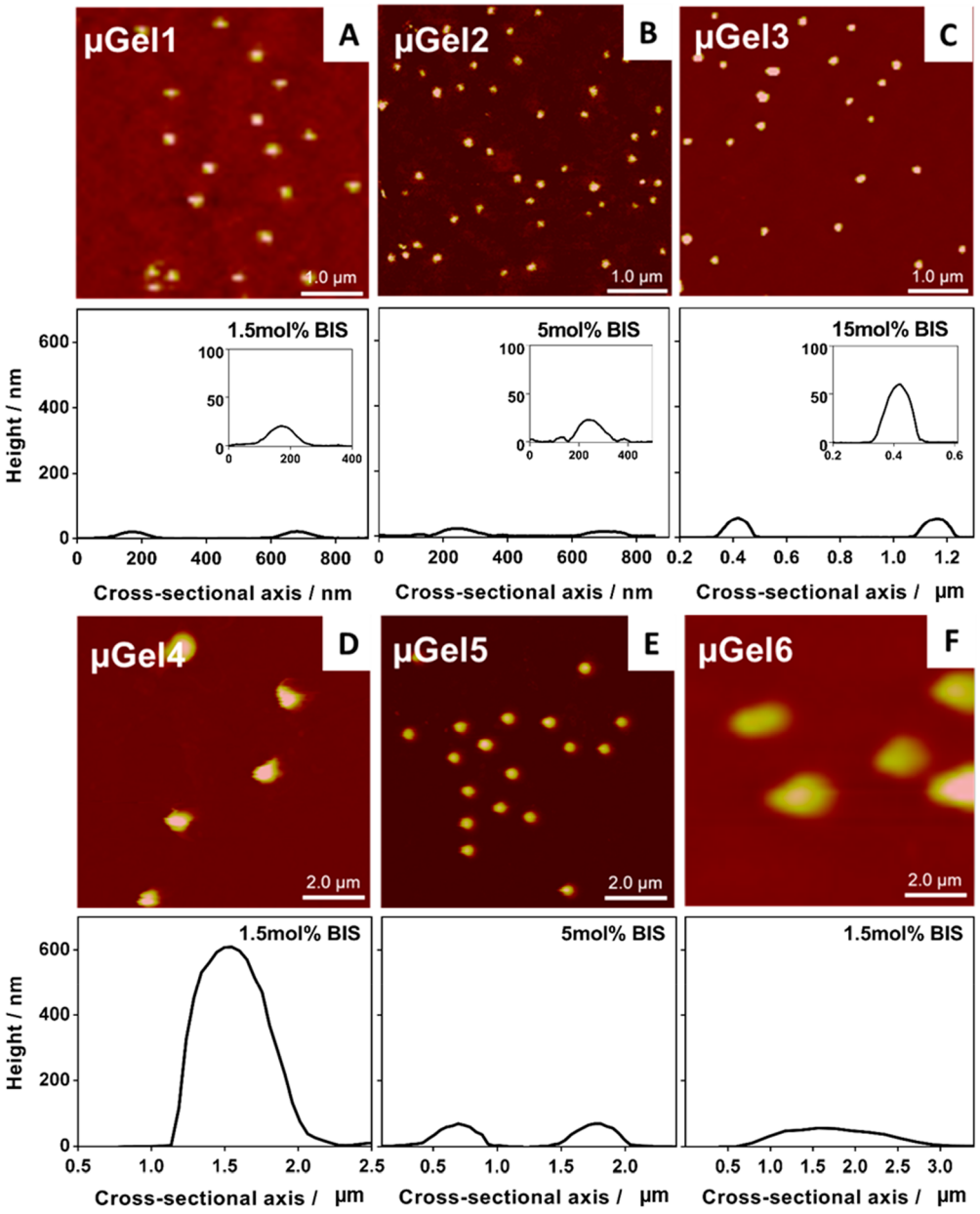

Figure 2. Atomic force microscopy images of single absorbed P(NIPMAM) microgels with different cross-linking densities onto silica wafer in wet state at 23 °C and corresponding representative height profiles across the apex of the absorbed μGels. The upper images represent the smaller microgels with similar R_h, but increasing stiffness form A (1.5 mol % BIS), B (5 mol % BIS), to C (15 mol % BIS), scale bar: 1 μm. Images at the bottom of panels D, E and F show in general larger particles (scale bar 2 μm) with different R_h values (depicted in Table 2) that provide variations in coating thickness and with altered internal cross-linking density also microgel stiffness.

adsorbed characteristics in terms of thickness. Further, the particles depicted in Figure 2A,D,F exhibit a similar cross-linking density but a gradual variation (from A over F to D) in coating thickness upon adsorption onto the surface. In general, the characteristics and deformability of the surface adsorbed

DOI: 10.1021/acs.biomac.8b01378
Biomacromolecules 2019, 20, 243−253

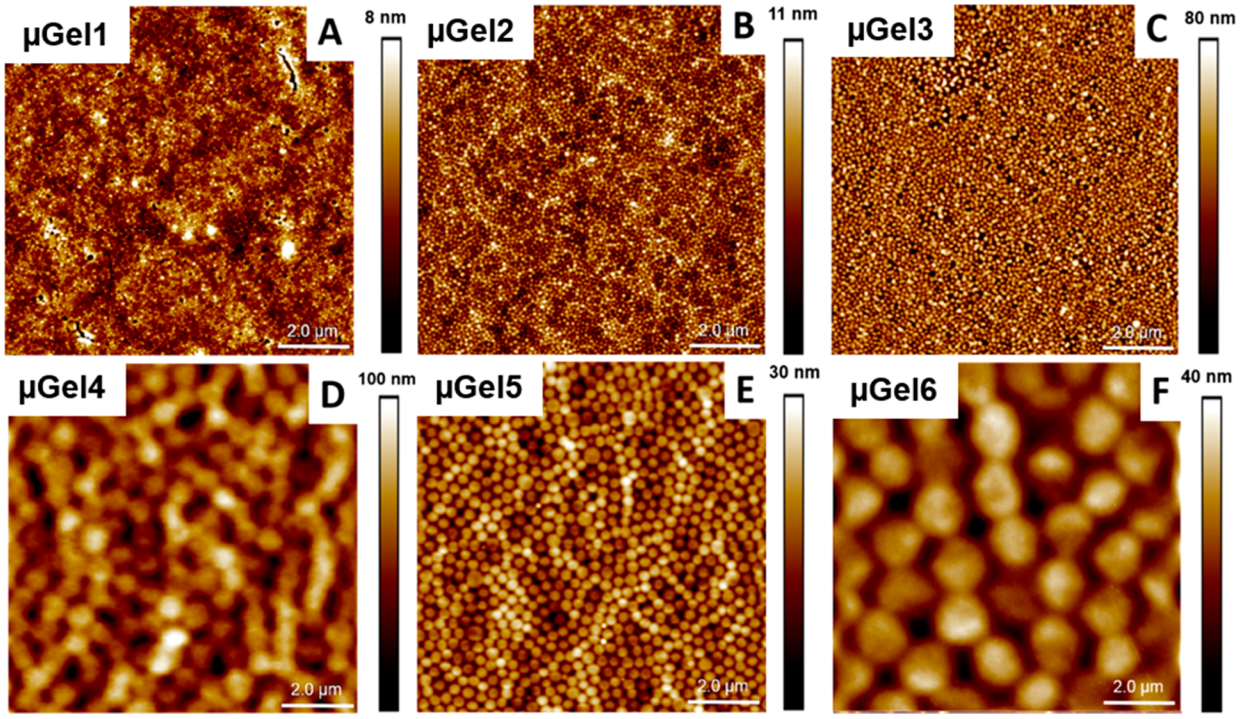

Figure 3. Atomic force microscopy images of the P(NIPMAM) microgel coated glass surfaces with different internal stiffness/cross-linking density and hydrodynamic radii R_h at 23 °C in the dry state. (A) μGel1, R_h = 114 nm, (B) μGel2, R_h = 109 nm, (C) μGel3, R_h = 101 nm, (D) μGel4, R_h = 787 nm, (E) μGel5, R_h = 301 nm, (F) μGel6, R_h = 650 nm at 30 °C.

particles is determined by the particle size and stiffness (Figure 1, S2, and Table 2).

Microgel-Based Coatings. In order to investigate the antifouling properties of the P(NIPMAM) microgel coating based on the particles described above, the negatively charged P(NIPMAM) microgels (see negative ζ-potentials, Table 2) were electrostatically adsorbed onto a PEI modified glass surface via spraying a microgel suspension onto the modified surface. The resulting microgel coated surfaces are depicted in Figure 3, in which panels A−C show AFM images of microgel coatings made of similar hydrodynamic radii, but increasing stiffness (see Table 2). In Figure 3D−F, AFM images of microgel coatings prepared of particles with larger R_h values are depicted. In Figure 3D (μGel 4) and F (μGel 6), coatings prepared from soft particles (1.5 mol % BIS) are shown, which is the same cross-linking density as for Figure 3A but with an increasing R_h. Based on the fuzzy surface of the particles at low cross-linking densities (Figure 3A,D,F) and due to spreading on the surface, the microgel structure in these images is less defined than the microgel structure of the stiffer coatings (Figure 3B,C,E). In all cases (Figure 3A−F), the microgel coating consists of a homogeneous monolayer, with a surface coverage of over 90%. The thickness of the coating was determined by surface scratching and evaluation of the height differences in dry state, exemplary shown for μGel 3 (R_h = 101 nm. 15 mol % BIS, see Figure S8). The height of the coating $h = 26 \pm 3$ nm is in good agreement with the height of the single absorbed microgel in dry state ($h = 31 \pm 8$ nm), confirming a microgel monolayer structure. For the soft microgel coatings (Figure 3A,D,F) some inhomogeneities could be observed, which are attributed to inhomogeneities within the adhesive PEI layer (see Figure S3). In Figure 3E, the microgel coating of the intermediate stiffness (5 mol % BIS, μGel 5) is depicted but with a larger R_h as used in Figure 3B, namely R_h = 114 nm (μGel 2, Figure 3B) versus R_h = 301 nm (μGel 5, Figure 3E).

Bacterial Adhesion on Microgel Coatings Affected by Layer Thickness and Stiffness. In order to understand the effect of P(NIPMAM) microgel cross-linking density, microgel size and layer thickness on bacterial adhesion, we used *S. aureus* ATCC 12600 in a parallel plate flow chamber system. Representative phase contrast microscopy images after 4 h bacterial adhesion for the uncoated and PEI coated glass slides as well as glass surfaces coated with microgels differing in cross-linking density are presented in Figure 4A. These images qualitatively show a decreased number of adhered bacteria on the microgel coated glass as compared to the bare glass and PEI coated glass controls. Hence, it can be concluded that microgel coatings are good candidates to prevent fouling.

In order to study quantitatively the effect of the microgel coating on bacterial adhesion, the number of adhering bacteria was determined by counting the number of bacteria on several spots on the substratum in three independent flow experiments (Figure 4B). The results demonstrate a significantly, almost 2 orders of magnitude, reduced number of adhering bacteria per unit area for all microgel coatings. Compared to bare glass surface, the reduction in number of adhering bacteria were 98%, 99% and 98% on the surfaces coated with microgels with 1.5, 5 and 15 mol % BIS cross-linking density, respectively. It is generally known that the antifouling properties of materials are connected with the formation of a hydration layer on the surface.[26,29] The water molecules adsorbed to the polymer layer form a physical and energetic barrier that hinders adhesion of the bacteria.[60] Microgels with their cross-linked, but porous networks can reach an extremely hydrated state, when swollen in aqueous media. Therefore, in addition to proteins and mammalian cells, bacteria are also efficiently repelled.[44,47] No significant difference is observed between the microgel coated

DOI: 10.1021/acs.biomac.8b01378
Biomacromolecules 2019, 20, 243−253

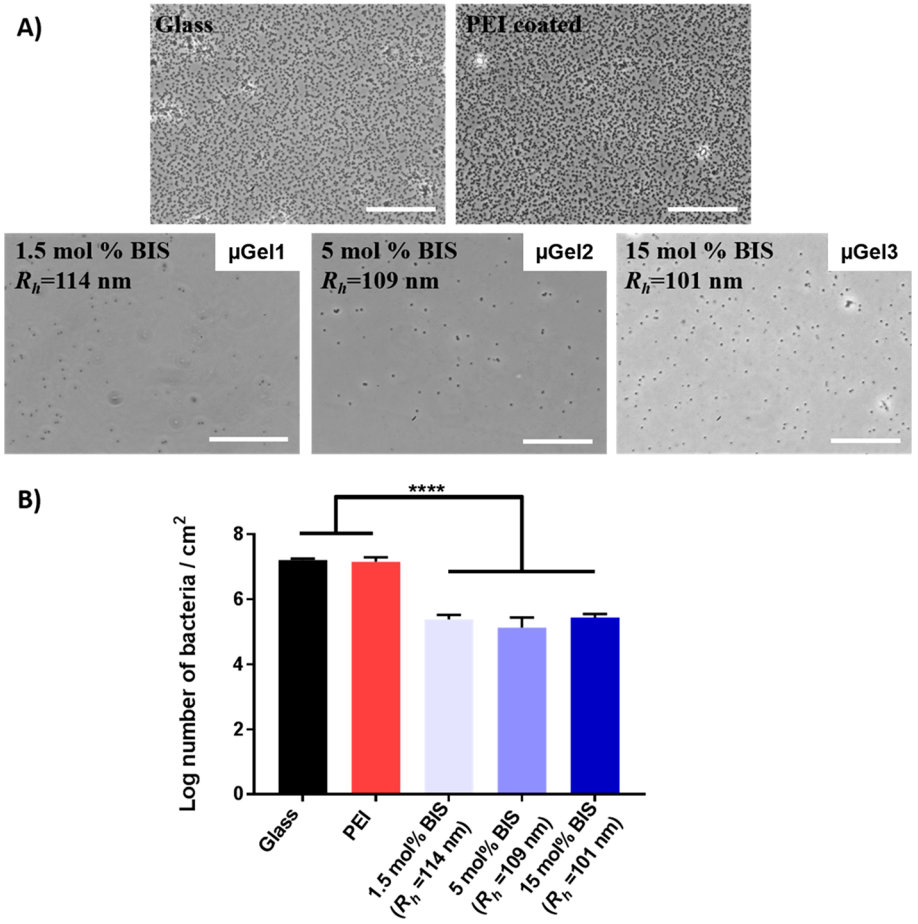

Figure 4. (A) Micrographs of *S. aureus* ATCC 12600 adhering after 4 h in a parallel plate flow chamber. Scale bar is 40 μm. (B) Number of bacteria adhering after 4 h on glass, PEI-coated glass, microgel ($R_h \cong 100$ nm each) coated glass with 1.5 mol % BIS, 5 mol % BIS, 15 mol % BIS cross-linking density. Statistically significant differences are indicated with **** (p <0.0001).

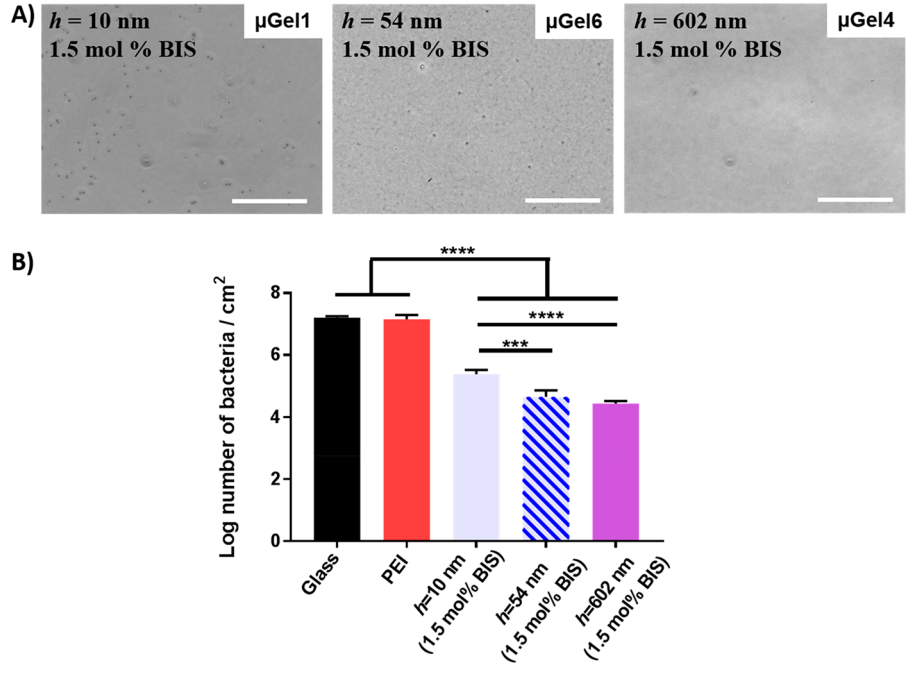

Figure 5. ((A) Micrographs of *S. aureus* ATCC 12600 adhering after 4 h in a parallel plate flow chamber. Scale bar is 40 μm. (B) Number of bacteria adhering after 4 h on glass, PEI-coated glass, microgel coated glass with the same cross-linking density (1.5 mol % BIS) but with different coating thicknesses as h = 10, 54 and 602 nm. Statistically significant differences are indicated with ** (p < 0.01) and **** (p < 0.0001).

DOI: 10.1021/acs.biomac.8b01378
Biomacromolecules 2019, 20, 243−253

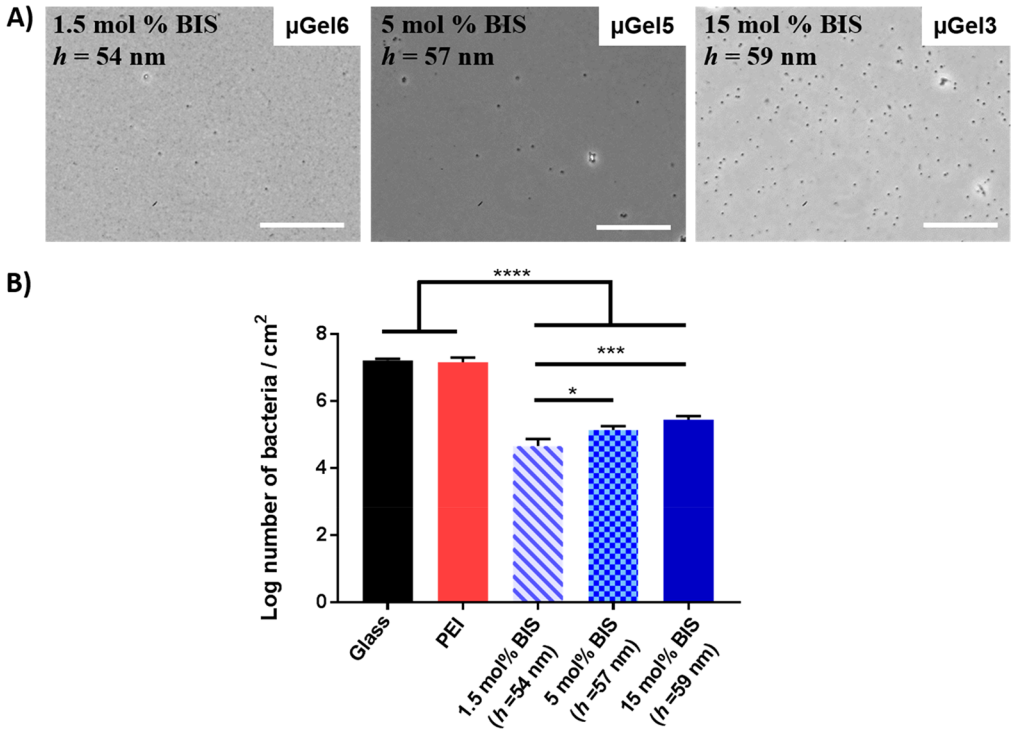

Figure 6. (A) Micrographs of *S. aureus* ATCC 12600 adhering after 4 h in a parallel plate flow chamber. Scale bar is 40 μm. (B) Number of bacteria adhering after 4 h on glass, PEI-coated glass, microgel coated glass with a cross-linking density of 1.5 mol % BIS (R_h = 650 nm), 5 mol % BIS (R_h = 301 nm) and 15 mol % BIS (R_h =101 nm), and a thickness h= 54−59 nm. Statistically significant differences are indicated with * ($p < 0.05$), *** ($p < 0.001$) and **** ($p < 0.0001$).

surfaces with different cross-linking densities. This shows that the particle stiffness analyzed here has no effect on the number of the adhering bacteria on the surface. Other systems showed that cell adhesion is reduced when the concentration of cross-linker incorporated into the microgel networks was increased.[29] However, in that study the microgels had a larger R_h and this may result in a thicker coating or altered surface roughness. Therefore, the surface morphology and roughness of the microgel coated samples were examined by AFM in the hydrated state to evaluate the effect of the surface roughness on adhesion behavior (see Figure S5). It is interesting to note the surface roughness of the samples, with the mean roughness values (R_a) are below 1.4 nm. These R_a results suggest that quite a low surface roughness range of 0.3−1.4 nm R_a is unlikely to influence the bacterial adhesion. It is remarkable that globular microgels produce a coating with an R_a of below 1.4 nm. We hypothesize that this flattening behavior occurs due to the drying step of the preparation method. During drying of the initially microgel multilayers, the microgels shrink and vacancies are produced between the microgels. Subsequently, microgels on top fill the spaces and form a film that is much denser than before. While rehydrating during washing that removes the multilayers, the particles swell. The high density of microgels result in a situation where the hydrodynamic diameter is larger than the interparticle distance resulting in the microgels being pushed into each other. The compression of the microgels result in reduced height features becoming more flattened (Figure S9). From our previous work using collagen hydrogel layers, the apparent stiffness is a combination from the substratum and thickness of the hydrogel layer.[61] It has been shown that the apparent stiffness of the layer also depends on the microstructure of the layer although, in the presented system this is unlikely as the over roughness of the hydrated microgel coating is in the low nanometer regime.[62] The thicker the layer, the lower the measured stiffness when a soft gel layer was applied to a hard substratum. Recent studies showed that decreasing the coating thickness on the substratum significantly increased the bacterial adhesion.[63,64] For this reason, the R_h of the microgel (μGel 1) was increased in order to form a thicker coating and identify if this increase would further influence the bacterial adhesion properties.

In order to examine the effect of the layer thickness on bacterial adhesion, we prepared microgel coatings with the same cross-linking density (1.5 mol % BIS) but different hydrodynamic radii, R_h (see Table 2 for microgel properties) and consequently three different microgel coating thicknesses for the surface absorbed state, with h = 10, 602 and 54 nm (see Figure 2, μGel1, μGel4 and μGel6). The microscopy images shown in Figure 5A display that all coatings prevent bacteria from adhering but that the thicker coatings (h = 54 nm and h = 602 nm) have a better antifouling property than the thinnest coating, purely owing to the thicker microgel coating as otherwise the microgel composition is the same. This finding illustrates that the substratum stiffness becomes an important factor when coatings are too thin. Although, the exact mechanism is not known how bacteria sense substrate stiffness, it is envisioned that bacteria on the microgel surface will deform the coating to some degree. If this deformation is larger than or in the same regime as the coating thickness, then the stiff substrate would be sensed by the bacteria as a stiffer substrate, which is in line with the increasing stiffness of the microgel being associated with higher number of adhered bacteria. Figure 5B illustrates the quantitative analysis and shows that bacterial adhesion is diminished with a decrease of around 99.8%, in case of the thickest microgel coating (h = 602 nm) compared to the bare glass. As there is a relative large contribution of the stiff

DOI: 10.1021/acs.biomac.8b01378
Biomacromolecules 2019, 20, 243−253

substratum when coatings are thin, difference in bacterial adhesion with respect to the different cross-linking densities might not be apparent. Therefore, different microgels were synthesized that form similar thick microgel coatings on the surface with varying cross-linking density. To achieve a similar layer thickness, the differently cross-linked microgels need to vary in R_h as they will have different deformability on the surface.

By controlling the size of the synthesized P(NIPMAM) microgels sprayed on the substrata, coatings with similar thickness of roughly h ∼ 60 nm were achieved while varying the microgel cross-linking densities. Figure 6 displays the bacterial adhesion on the different microgel coatings that are of similar thickness but differ in cross-linking density (1.5%, 5% and 15%). The microscopy images show that progressively more bacteria adhere on the stiffer microgel coatings (Figure 6A), which is supported by quantification of the number of bacteria (Figure 6B). The graph in Figure 6B indicates that the decrease in the number of bacteria adhered on the surface coated by microgels with 1.5 mol % BIS cross-linking density is 99.7% when compared to uncoated glass. It shows that the microgel with lowest cross-linking density prevents bacterial adhesion more than the surfaces coated by stiffer microgels while the coating thickness is equal. Besides, the effect of hydrogels with different cross-link density on mechanical interactions between bacteria and microgel coated surfaces might be related to coupled effect of stiffness and chemistry although the chemistry of the microgels, particularly at the surface, is highly similar among the different stiffnesses.[65] On the other hand, no significant differences were detected between 5 and 15 mol % BIS containing microgel coatings. Additionally, all microgel coatings exhibit excellent stability after flow chamber experiments as the coatings are still present and unaltered (see Figure S4).

Adhesion Kinetics: Unaffected by Microgel Coating Properties. The number of bacteria adhering per unit area after 4 h to the different coatings is much affected by the coating properties. In order to identify whether this is due to the initial rate of bacterial adhesion or the adhesion stability, adhesion kinetics were investigated. The initial deposition rate j_0 (cm^{-2} s^{-1}) was determined by monitoring the first 15 min of initial bacterial adhesion and the results are shown in Figure 7 of uncoated and PEI coated glass surface; and glass surface coated with different microgels. The results show that the initial adhesion rate of *S. aureus* ATCC 12600 is extremely reduced on the microgel coated surfaces. The initial deposition rate is reduced by 95% after the coating of microgels regardless the microgel or coating characteristics as compared to the control surfaces. There is no significant difference between the different microgel coated surfaces, indicating that the kinetics of initial bacteria adhesion is the same for all coatings. Therefore, the final resulting difference in number of bacteria adhering are most likely affected due to long-term differences in adhesion stability in which softer and thicker coatings exert different influences.

CONCLUSIONS

Our data show that adhesion of *S. aureus* ATCC 12600 on surfaces can be distinctly reduced by properly designed microgel coatings with respect to adhesion to glass controls. This, however, does not reveal a variance in reduced numbers of bacteria adhering onto microgel coated surfaces for different cross-linking densities of microgels when microgels have the same size. The size in solution does not reflect the size at the surface as upon microgel adsorption the different cross-linking densities will allow for different deformation, resulting in different coating thicknesses. Increasing the cross-linking density while keeping the coating layer thickness the same, resulted in higher number of bacterial adhesion on the surface. Hence, we can state that softer microgel coatings provide for better antifouling behavior. Additionally, a thicker microgel coating with the same stiffness will also allow for better antifouling behavior. The coatings were shown to be stable under experimental conditions as the microgel layer was still present after the flow experiments. While the final number of adhered bacteria per unit area differs for the different coatings, the initial deposition rate diminished up to 95% irrespective of the microgel coating characteristics. Hence, the initial adhesion kinetics are not influenced by microgel stiffness or coating thickness. In order to achieve different coating thicknesses, the size of the microgels were adjusted and ones adsorbed to the substratum, it may cause a difference in surface roughness. Although, due to the soft nature of the layers and their deformability, it is expected that it could have a minor contribution.

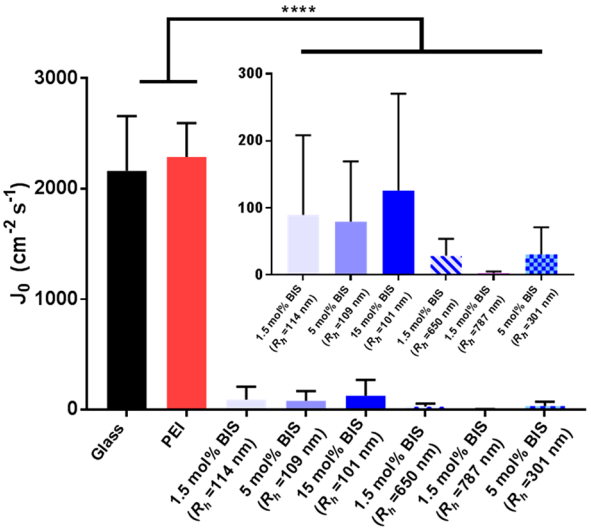

Figure 7. Initial deposition rates (j_0) of *S. aureus* ATCC 12600 on uncoated, PEI coated and microgel coated-glass surfaces. Statistically significant differences are indicated with **** ($p < 0.0001$).

It is expected that the strategy presented here can be employed to fabricate a variety of intelligent coating materials. After further development, a possible use of these smart microgel coating systems for biomedical applications (e.g., localized drug delivery, functional biomaterials and regenerative medicine) is envisioned.

ASSOCIATED CONTENT

Supporting Information

The Supporting Information is available free of charge on the ACS Publications website at DOI: 10.1021/acs.biomac.8b01378.

Additional figures of atomic force microscopy and dynamic light scattering along with technical details concerning the parallel flow setup for bacterial adhesion experiments (PDF)

AUTHOR INFORMATION

Corresponding Authors

*P. van Rijn. E-mail: p.van.rijn@umcg.nl.

DOI: 10.1021/acs.biomac.8b01378
Biomacromolecules 2019, 20, 243−253

*O. Mergel. E-mail: o.mergel@umcg.nl.

ORCID

Henny C. van der Mei: 0000-0003-0760-8900

Patrick van Rijn: 0000-0002-2208-5725

Funding

Olga Mergel gratefully acknowledges the Alexander von Humboldt Foundation for the Feodor Lynen Research Fellowship. Further the project leading to this publication has received funding from the European Union's Horizon 2020 research and innovation program under the Marie Skłodowska-Curie grant agreement No. 713482 (ALERT program).

Notes

The authors declare the following competing financial interest(s): H.J.B. also is director-owner of a consulting company, SASA BV.

■ ACKNOWLEDGMENTS

We thank Brandon W. Peterson for the help regarding statistical analysis. The project leading to this application has received funding from the Alexander von Humboldt Foundation and the European Union's Horizon 2020 research and innovation programme under the Marie Skłodowska-Curie grant agreement No 713482.

■ REFERENCES

(1) Arciola, C. R.; Campoccia, D.; Montanaro, L. Implant Infections: Adhesion, Biofilm Formation and Immune Evasion. *Nat. Rev. Microbiol.* **2018**, *16* (7), 397−409.

(2) Keskin, D.; Mokabbar, T.; Pei, Y.; van Rijn, P. The Relationship between Bulk Silicone and Benzophenone-Initiated Hydrogel Coating Properties. *Polymers* **2018**, *10* (5), 534.

(3) Magill, S. S.; Edwards, J. R.; Bamberg, W.; Beldavs, Z. G.; Dumyati, G.; Kainer, M. A.; Lynfield, R.; Maloney, M.; McAllister-Hollod, L.; Nadle, J.; et al. Multistate Point-Prevalence Survey of Health Care−Associated Infections. *N. Engl. J. Med.* **2014**, *370* (13), 1198−1208.

(4) Saini, H.; Chhibber, S.; Harjai, K. Antimicrobial and Antifouling Efficacy of Urinary Catheters Impregnated with a Combination of Macrolide and Fluoroquinolone Antibiotics against Pseudomonas Aeruginosa. *Biofouling* **2016**, *32* (5), 511−522.

(5) Wisniewski, N.; Reichert, M. Methods for Reducing Biosensor Membrane Biofouling. *Colloids Surf., B* **2000**, *18* (3), 197−219.

(6) Desai, T. A.; Hansford, D. J.; Leoni, L.; Essenpreis, M.; Ferrari, M. Nanoporous Anti-Fouling Silicon Membranes for Biosensor Applications. *Biosens. Bioelectron.* **2000**, *15* (9), 453−462.

(7) Seo, D. H.; Pineda, S.; Woo, Y. C.; Xie, M.; Murdock, A. T.; Ang, E. Y. M.; Jiao, Y.; Park, M. J.; Lim, S. IL; Lawn, M.; et al. Anti-Fouling Graphene-Based Membranes for Effective Water Desalination. *Nat. Commun.* **2018**, *9* (1), 683.

(8) Zhang, R.; Liu, Y.; He, M.; Su, Y.; Zhao, X.; Elimelech, M.; Jiang, Z. Antifouling Membranes for Sustainable Water Purification: Strategies and Mechanisms. *Chem. Soc. Rev.* **2016**, *45* (21), 5888−5924.

(9) Cabedo, L.; Gamez-Pérez, J. Inorganic-Based Nanostructures and Their Use in Food Packaging. In *Micro and Nano Technologies*; Cerqueira, M. Â. P. R., Lagaron, J. M., Pastrana Castro, L. M., de Oliveira Soares Vicente, A. A. M. B. T.-N., Eds.; Elsevier, 2018; Chapter 2, pp 13−45.

(10) Yebra, D. M.; Kiil, S.; Dam-Johansen, K. Antifouling Technology—past, Present and Future Steps towards Efficient and Environmentally Friendly Antifouling Coatings. *Prog. Org. Coat.* **2004**, *50* (2), 75−104.

(11) Sathe, P.; Laxman, K.; Myint, M. T. Z.; Dobretsov, S.; Richter, J.; Dutta, J. Bioinspired Nanocoatings for Biofouling Prevention by Photocatalytic Redox Reactions. *Sci. Rep.* **2017**, *7* (1), 3624.

(12) Ma, C.; Zhang, W.; Zhang, G.; Qian, P.-Y. Environmentally Friendly Antifouling Coatings Based on Biodegradable Polymer and Natural Antifoulant. *ACS Sustainable Chem. Eng.* **2017**, *5* (7), 6304−6309.

(13) Darouiche, R. O. Treatment of Infections Associated with Surgical Implants. *N. Engl. J. Med.* **2004**, *350* (14), 1422−1429.

(14) Costerton, J. W.; Stewart, P. S.; Greenberg, E. P. Bacterial Biofilms: A Common Cause of Persistent Infections. *Science* **1999**, *284* (5418), 1318−1322.

(15) Marine, J.; Myers, C. P.; Picquet, G. A.; Zaidel, L. A.; Wu, D.; Uhrich, K. E. Reduction of Bacterial Attachment on Hydroxyapatite Surfaces: Using Hydrophobicity and Chemical Functionality to Enhance Surface Retention and Prevent Attachment. *Colloids Surf., B* **2018**, *167*, 531−537.

(16) Singh, A. V.; Vyas, V.; Patil, R.; Sharma, V.; Scopelliti, P. E.; Bongiorno, G.; Podestà, A.; Lenardi, C.; Gade, W. N.; Milani, P. Quantitative Characterization of the Influence of the Nanoscale Morphology of Nanostructured Surfaces on Bacterial Adhesion and Biofilm Formation. *PLoS One* **2011**, *6* (9), No. e25029.

(17) Kao, W. K.; Gagnon, P. M.; Vogel, J. P.; Chole, R. A. Surface Charge Modification Decreases Pseudomonas Aeruginosa Adherence in Vitro and Bacterial Persistence in an in Vivo Implant Model. *Laryngoscope* **2017**, *127* (7), 1655−1661.

(18) Guégan, C.; Garderes, J.; Le Pennec, G.; Gaillard, F.; Fay, F.; Linossier, I.; Herry, J.-M.; Fontaine, M.-N. B.; Réhel, K. V. Alteration of Bacterial Adhesion Induced by the Substrate Stiffness. *Colloids Surf., B* **2014**, *114*, 193−200.

(19) Muszanska, A. K.; Rochford, E. T. J.; Gruszka, A.; Bastian, A. A.; Busscher, H. J.; Norde, W.; van der Mei, H. C.; Herrmann, A. Antiadhesive Polymer Brush Coating Functionalized with Antimicrobial and RGD Peptides to Reduce Biofilm Formation and Enhance Tissue Integration. *Biomacromolecules* **2014**, *15* (6), 2019−2026.

(20) Balamurugan, S.; Ista, L. K.; Yan, J.; López, G. P.; Fick, J.; Himmelhaus, M.; Grunze, M. Reversible Protein Adsorption and Bioadhesion on Monolayers Terminated with Mixtures of Oligo(Ethylene Glycol) and Methyl Groups. *J. Am. Chem. Soc.* **2005**, *127* (42), 14548−14549.

(21) Roosjen, A.; van der Mei, H. C.; Busscher, H. J.; Norde, W. Microbial Adhesion to Poly(Ethylene Oxide) Brushes:Influence of Polymer Chain Length and Temperature. *Langmuir* **2004**, *20* (25), 10949−10955.

(22) Ding, X.; Yang, C.; Lim, T. P.; Hsu, L. Y.; Engler, A. C.; Hedrick, J. L.; Yang, Y.-Y. Antibacterial and Antifouling Catheter Coatings Using Surface Grafted PEG-b-Cationic Polycarbonate Diblock Copolymers. *Biomaterials* **2012**, *33* (28), 6593−6603.

(23) Bearinger, J. P.; Terrettaz, S.; Michel, R.; Tirelli, N.; Vogel, H.; Textor, M.; Hubbell, J. A. Chemisorbed Poly(Propylene Sulphide)-Based Copolymers Resist Biomolecular Interactions. *Nat. Mater.* **2003**, *2*, 259.

(24) Keskin, D.; Clodt, J. I.; Hahn, J.; Abetz, V.; Filiz, V. Postmodification of PS-b-P4VP Diblock Copolymer Membranes by ARGET ATRP. *Langmuir* **2014**, *30* (29), 8907.

(25) Schoenfisch, M. H.; Pemberton, J. E. Air Stability of Alkanethiol Self-Assembled Monolayers on Silver and Gold Surfaces. *J. Am. Chem. Soc.* **1998**, *120* (18), 4502−4513.

(26) Chen, S.; Li, L.; Zhao, C.; Zheng, J. Surface Hydration: Principles and Applications toward Low-Fouling/Nonfouling Biomaterials. *Polymer* **2010**, *51* (23), 5283−5293.

(27) Schmidt, S.; Zeiser, M.; Hellweg, T.; Duschl, C.; Fery, A.; Möhwald, H. Adhesion and Mechanical Properties of PNIPAM Microgel Films and Their Potential Use as Switchable Cell Culture Substrates. *Adv. Funct. Mater.* **2010**, *20* (19), 3235−3243.

(28) Wang, S.; Zan, F.; Ke, Y.; Wu, G. Cells May Feel a Hard Substrate Even on a Grafted Layer of Soft Hydrogel. *J. Mater. Chem. B* **2018**, *6* (12), 1734−1743.

(29) Nolan, C. M.; Reyes, C. D.; Debord, J. D.; García, A. J.; Lyon, L. A. Phase Transition Behavior, Protein Adsorption, and Cell Adhesion Resistance of Poly(Ethylene Glycol) Cross-Linked Microgel Particles. *Biomacromolecules* **2005**, *6* (4), 2032−2039.

(30) Pelton, R. Temperature-Sensitive Aqueous Microgels. *Adv. Colloid Interface Sci.* **2000**, *85* (1), 1−33.

DOI: 10.1021/acs.biomac.8b01378
Biomacromolecules 2019, 20, 243−253

(31) Garcia, A.; Marquez, M.; Cai, T.; Rosario, R.; Hu, Z.; Gust, D.; Hayes, M.; Vail, S. A.; Park, C. Do Photo-, Thermally, and PH-Responsive Microgels. *Langmuir* **2007**, *23* (1), 224−229.
(32) Wong, J. E.; Richtering, W. Layer-by-Layer Assembly on Stimuli-Responsive Microgels. *Curr. Opin. Colloid Interface Sci.* **2008**, *13* (6), 403−412.
(33) Mergel, O.; Wünnemann, P.; Simon, U.; Böker, A.; Plamper, F. A. Microgel Size Modulation by Electrochemical Switching. *Chem. Mater.* **2015**, *27* (21), 7306−7312.
(34) Pankasem, S.; Thomas, J. K.; Snowden, M. J.; Vincent, B. Photophysical Studies of Poly(N-Isopropylacrylamide) Microgel Structures. *Langmuir* **1994**, *10* (9), 3023−3026.
(35) Fernández-Nieves, A.; Márquez, M. Electrophoresis of Ionic Microgel Particles: From Charged Hard Spheres to Polyelectrolyte-like Behavior. *J. Chem. Phys.* **2005**, *122* (8), 84702.
(36) Maccarrone, S.; Scherzinger, C.; Holderer, O.; Lindner, P.; Sharp, M.; Richtering, W.; Richter, D. Cononsolvency Effects on the Structure and Dynamics of Microgels. *Macromolecules* **2014**, *47* (17), 5982−5988.
(37) Zhao, W.; Nugroho, R. W. N.; Odelius, K.; Edlund, U.; Zhao, C.; Albertsson, A.-C. In Situ Cross-Linking of Stimuli-Responsive Hemicellulose Microgels during Spray Drying. *ACS Appl. Mater. Interfaces* **2015**, *7* (7), 4202−4215.
(38) Bromberg, L.; Alakhov, V. Effects of Polyether-Modified Poly(Acrylic Acid) Microgels on Doxorubicin Transport in Human Intestinal Epithelial Caco-2 Cell Layers. *J. Controlled Release* **2003**, *88* (1), 11−22.
(39) Bromberg, L.; Temchenko, M.; Hatton, T. A. Smart Microgel Studies. Polyelectrolyte and Drug-Absorbing Properties of Microgels from Polyether-Modified Poly(Acrylic Acid). *Langmuir* **2003**, *19* (21), 8675−8684.
(40) Farooqi, Z. H.; Khan, S. R.; Begum, R. Temperature-Responsive Hybrid Microgels for Catalytic Applications: A Review. *Mater. Sci. Technol.* **2017**, *33* (2), 129−137.
(41) Giaquinto, M.; Micco, A.; Aliberti, A.; Ricciardi, A.; Ruvo, M.; Cutolo, A.; Cusano, A. Microgel Photonics and Lab on Fiber Technology for Advanced Label-Free Fiber Optic Nanoprobes. *Sixth European Workshop on Optical Fibre Sensors (EWOFS'2016)*, Limerick, Ireland, 2016; SPIE, Vol. *9916*, 99161M.
(42) Microgel-Based Thermo-Responsive Membranes for Water Filtration. *Membr. Technol.* **2014**, *2014* (8) 10, DOI: .
(43) Sigolaeva, L. V.; Gladyr, S. Y.; Gelissen, A. P. H.; Mergel, O.; Pergushov, D. V.; Kurochkin, I. N.; Plamper, F. A.; Richtering, W. Dual-Stimuli-Sensitive Microgels as a Tool for Stimulated Spongelike Adsorption of Biomaterials for Biosensor. *Biomacromolecules* **2014**, *15* (10), 3735−3745.
(44) Wei, J.; Cai, J.; Li, Y.; Wu, B.; Gong, X.; Ngai, T. Investigation of Cell Behaviors on Thermo-Responsive PNIPAM Microgel Films. *Colloids Surf., B* **2015**, *132*, 202−207.
(45) Rose, J. C.; Gehlen, D. B.; Haraszti, T.; Köhler, J.; Licht, C. J.; De Laporte, L. Biofunctionalized Aligned Microgels Provide 3D Cell Guidance to Mimic Complex Tissue Matrices. *Biomaterials* **2018**, *163*, 128−141.
(46) Saxena, S.; Spears, M. W., Jr.; Yoshida, H.; Gaulding, J. C.; García, A. J.; Lyon, L. A. Microgel Film Dynamics Modulate Cell Adhesion Behavior. *Soft Matter* **2014**, *10* (9), 1356−1364.
(47) Scott, E. A.; Nichols, M. D.; Cordova, L. H.; George, B. J.; Jun, Y.-S.; Elbert, D. L. Protein Adsorption and Cell Adhesion on Nanoscale Bioactive Coatings Formed from Poly(Ethylene Glycol) and Albumin Microgels. *Biomaterials* **2008**, *29* (34), 4481−4493.
(48) Cross, M. C.; Toomey, R. G.; Gallant, N. D. Protein-Surface Interactions on Stimuli-Responsive Polymeric Biomaterials. *Biomed. Mater.* **2016**, *11* (2), 22002.
(49) Liu, Y.; Xing, L.; Zhang, Q.; Mu, Q.; Liu, P.; Chen, K.; Chen, L.; Zhang, X.; Wang, K.; Wei, Y. Thermo- and Salt-Responsive Poly(NIPAm-Co-AAc-Brij-58) Microgels: Adjustable Size, Stability under Salt Stimulus, and Rapid Protein Adsorption/Desorption. *Colloid Polym. Sci.* **2016**, *294* (3), 617−628.
(50) Ji, H.; Xiong, L.; Shi, Z.; He, M.; Zhao, W.; Zhao, C. Engineering of Hemocompatible and Antifouling Polyethersulfone Membranes by Blending with Heparin-Mimicking Microgels. *Biomater. Sci.* **2017**, *5* (6), 1112−1121.
(51) Vatankhah-Varnosfaderani, M.; Hu, X.; Li, Q.; Adelnia, H.; Ina, M.; Sheiko, S. S. Universal Coatings Based on Zwitterionic−Dopamine Copolymer Microgels. *ACS Appl. Mater. Interfaces* **2018**, *10* (24), 20869−20875.
(52) Nyström, L.; Malmsten, M. Surface-Bound Microgels — From Physicochemical Properties to Biomedical Applications. *Adv. Colloid Interface Sci.* **2016**, *238*, 88−104.
(53) Kolewe, K. W.; Zhu, J.; Mako, N. R.; Nonnenmann, S. S.; Schiffman, J. D. Bacterial Adhesion Is Affected by the Thickness and Stiffness of Poly(Ethylene Glycol) Hydrogels. *ACS Appl. Mater. Interfaces* **2018**, *10* (3), 2275−2281.
(54) Kolewe, K. W.; Peyton, S. R.; Schiffman, J. D. Fewer Bacteria Adhere to Softer Hydrogels. *ACS Appl. Mater. Interfaces* **2015**, *7* (35), 19562−19569.
(55) Ballauff, M.; Lu, Y. Smart" Nanoparticles: Preparation, Characterization and Applications. *Polymer* **2007**, *48* (7), 1815−1823.
(56) Kumar, A.; Srivastava, A.; Galaev, I. Y.; Mattiasson, B. Smart Polymers: Physical Forms and Bioengineering Applications. *Prog. Polym. Sci.* **2007**, *32* (10), 1205−1237.
(57) Roosjen, A.; Kaper, H. J.; van der Mei, H. C.; Norde, W.; Busscher, H. J. Inhibition of Adhesion of Yeasts and Bacteria by Poly(Ethylene Oxide)-Brushes on Glass in a Parallel Plate Flow Chamber. *Microbiology* **2003**, *149* (11), 3239−3246.
(58) Busscher, H. J.; van der Mei, H. C. Microbial Adhesion in Flow Displacement Systems. *Clin. Microbiol. Rev.* **2006**, *19* (1), 127−141.
(59) Von Nessen, K.; Karg, M.; Hellweg, T. Thermoresponsive Poly-(N-Isopropylmethacrylamide) Microgels: Tailoring Particle Size by Interfacial Tension Control. *Polymer* **2013**, *54* (21), 5499−5510.
(60) Fang, F.; Satulovsky, J.; Szleifer, I. Kinetics of Protein Adsorption and Desorption on Surfaces with Grafted Polymers. *Biophys. J.* **2005**, *89* (3), 1516−1533.
(61) Vasse, G. F.; Kühn, P. T.; Zhou, Q.; Bhusari, S. A.; Reker-Smit, C.; Melgert, B. N.; van Rijn, P. Collagen Morphology Influences Macrophage Shape and Marker Expression in Vitro. *J. Immunol. Regen. Med.* **2018**, *1*, 13−20.
(62) Duan, P.; Toumpaniari, R.; Partridge, S.; Birch, M. A.; Genever, P. G.; Bull, S. J.; Dalgarno, K. W.; McCaskie, A. W.; Chen, J. How Cell Culture Conditions Affect the Microstructure and Nanomechanical Properties of Extracellular Matrix Formed by Immortalized Human Mesenchymal Stem Cells: An Experimental and Modelling Study. *Mater. Sci. Eng., C* **2018**, *89*, 149−159.
(63) Kolewe, K. W.; Zhu, J.; Mako, N. R.; Nonnenmann, S. S.; Schiffman, J. D. Bacterial Adhesion Is Affected by the Thickness and Stiffness of Poly(Ethylene Glycol) Hydrogels. *ACS Appl. Mater. Interfaces* **2018**, *10* (3), 2275−2281.
(64) Yadav, V.; Jaimes-Lizcano, Y. A.; Dewangan, N. K.; Park, N.; Li, T.-H.; Robertson, M. L.; Conrad, J. C. Tuning Bacterial Attachment and Detachment via the Thickness and Dispersity of a PH-Responsive Polymer Brush. *ACS Appl. Mater. Interfaces* **2017**, *9* (51), 44900−44910.
(65) Kandemir, N.; Vollmer, W.; Jakubovics, N. S.; Chen, J. Mechanical Interactions between Bacteria and Hydrogels. *Sci. Rep.* **2018**, *8* (1), 10893.

DOI: 10.1021/acs.biomac.8b01378
Biomacromolecules 2019, 20, 243−253